# Does the Influence of Oblate-Like Distortions in Larger Raindrops Make a Difference in Collection and Evaporation Parameterizations?

JERRY M. STRAKA

*School of Meteorology, University of Oklahoma, Norman, Oklahoma*

MATTHEW S. GILMORE

*Department of Atmospheric Sciences, University of Illinois at Urbana–Champaign, Urbana, Illinois*

(Manuscript received 15 June 2005, in final form 10 March 2006)

ABSTRACT

This note documents the results of more exact parameterizations for continuous-collection growth and evaporation against simpler traditional ones. Although the main focus is on improving research models, the research results also apply to high-resolution forecast models because the use of lookup tables can make the proposed evaporation, terminal velocity, and collection parameterizations as fast as or faster than proposed ones. It is shown that the older method of ignoring oblate-like distortions of shapes in raindrops, truncated at a maximum diameter of 8 mm, gives a solution like that including oblate-like distortions but only because of two large errors that nearly cancel. The biggest differences from the solutions using oblate-like distortions in shape arise from parameterizations that incorporate more exact approximations (e.g., sweep-out diameter) that are not combined with appropriately more exact approximations for other variables dependent on diameter (e.g., terminal velocity).

## 1. Introduction

Although it is well known that raindrops become increasingly oblate-like for diameters greater than 1 mm (e.g., Pruppacher and Pitter 1971; hereinafter PP71) owing to surface tension and drag force, the potentially important influence of shape distortion has yet to be parameterized and tested for use in at least research cloud models. Rather than the oblate-like "footprint" diameter $D_{ob}$, the smaller equivalent diameter $D_{eq}$ has been used exclusively when raindrops collect other particles. Furthermore, an accurate representation of the effect of oblate-like shape distortion on raindrop terminal fall velocities has not been typically well represented by power laws in most cloud models. The purposes of this paper are to evaluate more exact raindrop continuous-collection parameterization equation and raindrop evaporation equation that account for raindrop oblate-like shape distortions in drop geometry and more accurate terminal velocity relationships. (As shown later, volume-preserving parameterizations based on $D = ab^2$, where $a$ and $b$ are the minor and major axis, respectively, are too difficult to integrate and thus their use is too difficult to evaluate.)

Equivalent diameter $D_{eq}$ has traditionally been used for raindrop collection of cloud drops, drizzle drops, other raindrops, and other particles in cloud models. Using $D_{eq}$ is reasonable for $D_{ob} \leq 1$ mm (PP71) because drops these sizes naturally assume spherical shapes while falling, owing to surface tension. Using $D_{eq}$ for $1 \leq D_{ob} \leq 4$ mm may be slightly less acceptable because, although such particles are nearly spherical in the time mean owing to oscillations (Andsager et al. 1999), in situ snapshots from video show highly distorted drops in this size range (Bringi and Chandrasekar 2000).

As $D_{eq}$ increases from 4 mm, the raindrops are continuously more oblate-like in shape, with aspect ratios approaching 0.6–0.5 as drops approach 8 mm, or slightly more, in diameter. This shape distortion should unambiguously increase the geometric sweep-out area (Fig. 1) and decrease terminal fall velocity (Gunn and Kinzer 1949; Beard and Pruppacher 1969; PP71) relative to an equivalent spherical raindrop. It is admitted

*Corresponding author address:* Jerry M. Straka, School of Meteorology, University of Oklahoma, 100 E. Boyd St., Norman, OK 73019.
E-mail: jstraka@ou.edu

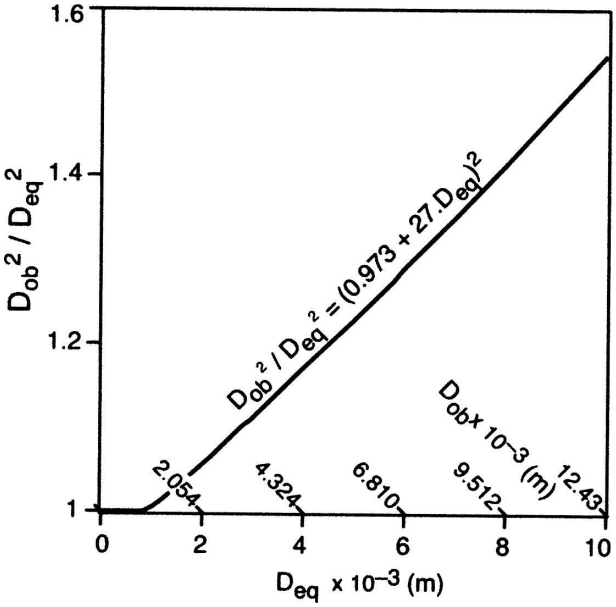


FIG. 1. Ratio of the sweep-out areas between an oblate-like distorted raindrop and its corresponding equivalent sphere using the relationship from Beard (1976). The $D_{eq}$ and $D_{ob}$ are both shown on the $x$ axis.

that oblate-like shape distortions could be limited there because raindrops become less frequent at larger sizes because of breakup owing to both drop collisions ($D_{eq} \geq 4$ mm) and hydrodynamic instability (roughly $D_{eq} \geq 8$–8.5 mm). A fairly complete discussion of potential maximum sizes is discussed in PP71 and Pruppacher and Klett (1997). However, despite these breakup mechanisms that might keep raindrops small and reduce oblateness, there are excellent in situ observations by Rauber et al. (1991) from shallow Hawaiian clouds that show that a large number of oblate-like raindrops ($3 \leq D_{eq} \leq 8$ mm) can occur, albeit rarely, in at least some cases. Moreover melting hail may become largely liquid with a small ice core and be very oblate in shape (Bringi and Chandrasekar 2000). Therefore, raindrop oblate-like shape distortions may be an important characteristic to parameterize in high-resolution cloud models with complex (bulk parameterized or bin) microphysics. They may also be important in larger-scale models with detailed microphysical parameterizations, especially if a fallout equation is used and more accurate vertical flux is required.

In section 2 the analysis method and derivations of four different continuous-collection growth equations are presented. Then, inclusion of drop distortion into the evaporation equation is described. Section 3 presents numerical results and a discussion of idealized computations of the equations presented in the section 2. In section 4 the results of the paper are summarized.

## 2. Analysis

Because the oblate-like shape distortion effect of having increased geometric sweep-out area (increased sweep-out volume and thus accretion rate) competes against the oblate-like distortion shape effect of having decreased terminal fall velocity (decreased sweep-out rate and accretion rate), it is necessary to evaluate these two effects of oblateness both individually and together, in simple numerical experiments. This approach can be achieved by analyzing four different versions of the continuous-collection growth equation. The first equation to be derived is in every way similar to Lin et al. (1983, hereinafter LFO83), except that it is generalized for any gamma distribution and allows integration to a maximum rain diameter $D_{max}$. It does not include the effects of oblate-like shape distortions for raindrops, and such an exclusion is common practice in both bulk and bin models. The second equation to be derived is the same as the first except that it includes the effect of oblate-like shape distortions increasing the geometric sweep-out area only. The third equation to be derived is the same as the first except that it includes the effect of oblate-like shape distortions on reducing the terminal velocity term only by using an accurate third-order polynomial to fit the empirical data. The fourth equation to be derived, which is the accretion equation that should be most realistic, includes the combined effects of oblate-like shape distortions on both increasing the geometric sweep out as well as reducing the maximum terminal velocity.

The fifth and sixth equations to be derived are for evaporation without and with oblate-like distortions for diameter and the third-order terminal velocity approximation discussed herein. After these equations are derived and discussed, some simple numerical experiments are performed to demonstrate the differences in approaches (section 3).

In every case, the collector raindrops are represented with a generalized partial gamma distribution and the collected cloud droplets are represented as being monodisperse. To make a fair comparison, the partial gamma distributions only contain raindrops between 0 mm and a maximum allowed raindrop diameter $D_{max}$ of 8 mm.

### *a. The Lin et al. (1983) continuous-collection growth equation for a generalized gamma distribution*

LFO83 approximated the continuous-collection growth of rain (subscript $r$) collecting cloud water (subscript $c$) with

$$dq_r/dt = \int_0^{D_{\max}} \pi(D_r/2)^2 V_{Tr}(D_r) E_{r,c} q_c n_r(D_r)\, dD_r, \tag{1}$$

by assuming $D_r \gg D_c$ and $V_{Tr} \gg V_{Tc}$. Here, $D_r$ is equivalent volume rain diameter, $V_{Tr}$ is rain terminal velocity, $E_{r,c}$ is collection efficiency, $q_c$ is cloud water mixing ratio, and $n_r(D_r)$ is the spectral density function for rain. (Hereinafter, the $r$ subscript will be dropped wherever possible for simplicity such that only cloud water variables are subscripted.) Then, LFO83 assumed

$$V_T = aD^b(\rho_{oo}/\rho_o)^{0.4}, \tag{2}$$

where $a$ (units: $\mathrm{m}^{1-b}\ \mathrm{s}^{-1}$) and $b$ (dimensionless) are parameters and $\rho_o$ and $\rho_{oo}$ are the air density and reference air density ($\rho_{oo} = 1.225\ \mathrm{kg\ m}^{-3}$), respectively. Although LFO83 originally used an exponent of 0.5, an exponent of 0.4 is recommended by K. V. Beard (2006, personal communication), and thus we use that throughout. Also, $a = 842\ \mathrm{m}^{1-b}\ \mathrm{s}^{-1}$ and $b = 0.8$ (Liu and Orville 1969, hereinafter LO69; LFO83). Instead of assuming an inverse exponential distribution, however, we choose distribution moments and spectral density function parameters that follow Walko et al. (1995) but are modified to allow a $D_{\max}$ of less than $\infty$ (see the appendix). The following intermediate expression appears after substituting the gamma distribution for the spectral density function (A1) along with (2),

$$\frac{dq}{dt} = \frac{a\pi E N_t q_c}{4\Gamma(\nu)} D_n^{2+b}\left(\frac{\rho_{oo}}{\rho_o}\right)^{0.4} \int_0^{D_{\max}} \left(\frac{D}{D_n}\right)^{2+b}\left(\frac{D}{D_n}\right)^{\nu-1} \exp\left(-\frac{D}{D_n}\right) d\left(\frac{D}{D_n}\right); \tag{3}$$

$E$ is the collection efficiency and is set to unity (following LFO83). The variable $q_c$ is cloud water mixing ratio, and $N_t$ is total number of raindrops. Integrating from 0 to $D_{\max}$ gives

$$\frac{dq}{dt} = \frac{a\pi E N_t q_c}{4\Gamma(\nu)}\left[\gamma\left(2 + b + \nu, \frac{D_{\max}}{D_n}\right) D_n^{2+b}\right]\left(\frac{\rho_{oo}}{\rho_o}\right)^{0.4}, \tag{4}$$

where an equation for the characteristic diameter $D_n$ is given in the appendix and where $\gamma(2 + b + \nu, D_{\max}/D_n)$ represents the partial gamma function integrated between 0 and $D_{\max}$. Assuming no breakup or self-collection, $N_t$ remains constant. For now (4) will be called the traditional continuous-collection growth scheme following LFO83 or just the "LFO" or the "LFO83 scheme," but it will be understood that it has been generalized/modified to handle any gamma distribution (i.e., any shape parameter) and any $D_{\max}$. For our comparisons we chose $D_{\max} = 8$ mm although all other models use $D_{\max} = \infty$ when they use this equation.

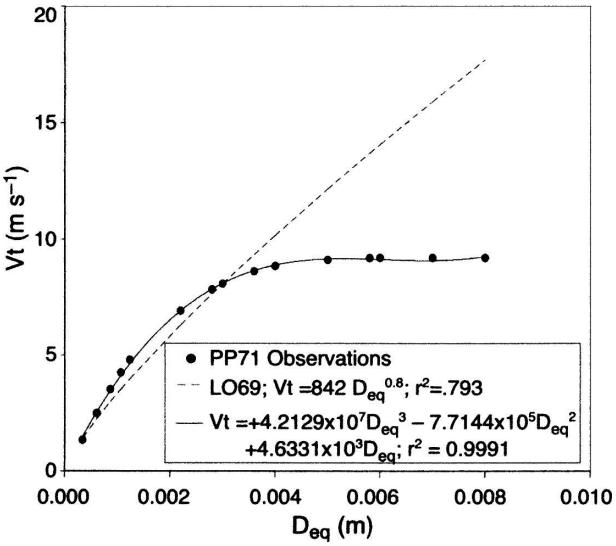


FIG. 2. From Gunn and Kinzer (1949) and Beard and Pruppacher (1969), and presented by PP71, are laboratory data of $V_T$ ($\mathrm{m\ s}^{-1}$) vs $D_{\mathrm{eq}}$ (m), our proposed third-order polynomial fit, and the LO69 power-law fit of $V_T$ vs $D_{\mathrm{eq}}$ (originally fitted for $D < 5$ mm; plotted here to 8 mm). Equations and $r^2$ values (relative to PP71 data up to $D_{\mathrm{eq}} = 8$ mm) are shown in the legend along with the line styles.

Note again that (4) assumes an equivalent volume diameter $D_{\mathrm{eq}}$ for both the collection sweep-out area and in the power law for $V_T$. It is obvious that $D_{\mathrm{eq}} \leq$ the oblate-like footprint diameter $D_{\mathrm{ob}}$, and thus the sweep-out area should be less than reality in this traditional scheme. However, we will now show that $V_T(D_{\mathrm{eq}})$ is very high owing to the use of the LO69/LFO83 approximation and this counteracts the smaller sweep-out area in the accretion rate.

LO69 used the least squares method to fit the laboratory data tabulated by Gunn and Kinzer (1949) for $D <$ 3–4 mm. Although the LO69 power law can be used to predict the PP71 raindrop $V_T$ data (originally from Gunn and Kinzer 1949 and Beard and Pruppacher 1969) well at small diameters ($D <$ 3–4 mm), it reveals a correlation of only 0.793 if $D_{\mathrm{eq}}$ is extrapolated to 8 mm. This is because LO69 (and LFO83-like schemes that use the same method) do not capture the reduction in terminal velocity resulting from oblate-like shape distortions for $D_{\mathrm{eq}} >$ 3–4 mm (Fig. 2). In the extreme, LO69/LFO raindrop $V_T$ estimates are nearly 2 times as

large as they should be at 8 mm and get worse for larger diameters when compared with observations. This poses a potential problem because many LFO83-like models using LO69 integrate $D$ to $\infty$ in their collection equations (e.g., LFO83; Reisner et al. 1998; Gilmore et al. 2004; Thompson et al. 2004). Thus, for large raindrops, the LO69/LFO83 version of $V_T$ is overestimated relative to the observations.

### b. *Continuous-collection growth equation with an oblate-like shape distortion correction for geometric sweep-out area*

Now the influence of using oblate-like distorted drop diameters instead of the equivalent diameter drop (Fig. 1) in the geometric sweep-out area ($\pi/4D^2$) of the geometric sweep-out volume ($\pi/4D^2V_T\Delta t$) for the continuous-collection growth equation is examined, where $D_{ob}$ is actual drop footprint diameter, $V_T$ is drop terminal velocity, and $t$ is time. In the LFO83 version shown in (4), and in all other models of which we are aware, this influence is not accounted for. The area swept out by an actual raindrop with $D_{ob}$ is quite a bit more than $D_{eq}$ and exceeds 1.4 times near the hydrodynamic breakup diameter (Fig. 1). (In Fig. 3 of PP71, it was shown in that there was a change in aspect ratio and deviation from $D_{eq}$ by a factor nearly as large as 0.5–0.6 at $D$ approaching the hydrodynamic breakup diameter limit.) To accommodate for this difference, a polynomial from Beard (1976) was used to write the observed $D_{ob}$ in terms of $D_{eq}$:

$$D_{ob} = A_1 D_{eq} + A_2 D_{eq}^2, \tag{5}$$

where $A_1 = 0.973$ (dimensionless) and $A_2 = 27\ \mathrm{m}^{-1}$, and a fit to the PP71 data shows a correlation of near 1.0. Beard (1976) notes that this equation is meant for $D > 1$ mm, but we have found that it also performs well (in giving $D_{eq} \approx D_{ob}$, as it should) for $D < 1$ mm.

Because our derivation includes the oblate-like shape distortions in diameter, the polynomial relationship in (5) is substituted for $D_{ob}$ prior to integration over $D_{eq}$. (One could also integrate over $D_{ob}$ if the model equations were written in such a form.) Thus, following the same derivation as in (4) except using empirical raindrop diameters [(5)] in the sweep-out area, one arrives at

$$\frac{dq}{dt} = \frac{a\pi E N_t q_c}{4\Gamma(\nu)} f_1 \left(\frac{\rho_{oo}}{\rho_o}\right)^{0.4}, \tag{6}$$

where

$$f_1 = +A_1^2\gamma\left(2 + b + \nu, \frac{D_{\max}}{D_n}\right)D_n^{2+b} + 2A_1A_2\gamma\left(3 + b + \nu, \frac{D_{\max}}{D_n}\right)D_n^{3+b} + A_2^2\gamma\left(4 + b + \nu, \frac{D_{\max}}{D_n}\right)D_n^{4+b}. \tag{7}$$

Here $\gamma$ represents the partial gamma function integrated between 0 and $D_{\max}$.

One of the reviewers suggested that instead of (7) one could use the volume constraint for an oblate spheroid ($D_{eq}^3 = ab^2$) and combine that with an axis ratio relationship such as from Pruppacher and Beard's (1970) wind-tunnel measurements: $b/a = (1.03 + 0.62D_{eq})$. Solving for the oblate spheroid major axis $b$ results in $b = D_{eq}/(1.03 + 0.62D_{eq})^{-1/3}$, and that can be substituted for $D$ in (1), giving

$$\frac{dq_r}{dt} = \int_0^{D_{\max}} 0.25\left[\pi \frac{D_{eq}}{(1.03 + 0.62D_{eq})^{-1/3}}\right] \times Vt(D_r)E_{r,c}q_c n(D_r)\, dD_r.$$

However, this is far too difficult to integrate as compared with (6) and (7) shown above. Furthermore, because the above expression invokes the unnecessary assumption that the raindrops are perfect oblate spheroids ($b < D_{ob}$), it artificially reduces the accretion rates in comparison with the entirely empirical form shown in (6) and (7). For these reasons, we advocate using $D_{ob}$ instead of $b$ in (1) when accounting for oblate-like drop distortions.

Last, K. V. Beard (2006, personal communication) has provided "that the change in axis ratio with altitude is expected to be negligible when the distorting effect of an increased terminal velocity is compensated by decreased air density. According to the perturbation model (Beard et al. 1989) the distortion is proportional to the Weber number, a product of the air density and fall speed squared. *If* the fall speed is proportional to the square root of the air density—the usual assumption—the Weber number and therefore distortion do not change."

### c. *Continuous-collection growth equation with oblate-like distortion corrections for terminal velocity only*

We found much better fits to $V_T(D_{eq})$ from Gunn and Kinzer 1949, Beard and Pruppacher (1969), and PP71 by using third-, fourth-, and fifth-order polynomi-

als[1] than was found for LO69's power-law fit; the following is the third-order fit that has a correlation of a bit better than 0.9991 and does a much better job for the larger drops:

$$V_T(D_{\rm ob}) = (B_1 D_{\rm eq} + B_2 D_{\rm eq}^2 + B_3 D_{\rm eq}^3)\left(\frac{\rho_{oo}}{\rho_o}\right)^{0.4}, \tag{8}$$

where $B_1 = 4.633\ 08 \times 10^3\ {\rm s}^{-1}$, $B_2 = -7.7144 \times 10^5\ {\rm m}^{-1}\ {\rm s}^{-1}$, and $B_3 = 4.2129 \times 10^7\ {\rm m}^{-2}\ {\rm s}^{-1}$. Recall that LO69 had a correlation of only about 0.793. A plot of (8) produces a very good match to the data (Fig. 2) and tends to about 9.2 m s$^{-1}$ for sea level conditions out toward 8 mm, as it should. Both (2) and (8) both provide good estimates for $D_{\rm eq} < 3$ or 4 mm, but (8) greatly improves the terminal velocity estimates for $D_{\rm eq} > 3$ or 4 mm relative to LO69. Scheme (8) is well behaved out to a $D_{\rm eq}$ of 8 mm, with only very weak oscillatory behavior that is slightly detectable in the plot starting at diameters of $D_{\rm eq}$ of >6 mm or so (Fig. 2). However, it does begin to fail some at very large diameters (not shown), where observed rain number concentrations approach zero or are zero (Pruppacher and Klett 1997). Because of this result, a $D_{\rm max}$ of 8 mm must be imposed in the accretion equation to follow below. This imposition is all right, because this value is typically the largest drop size observed.

Using the gamma distribution function (e.g., see the appendix) and the continuous-collection growth rate assuming (8) for terminal velocity yields

$$\frac{dq}{dt} = \frac{\pi E N_t q_c}{4\Gamma(\nu)} f_2 \left(\frac{\rho_{oo}}{\rho_o}\right)^{0.4}, \tag{9}$$

where

$$f_2 = B_1 \gamma\left(3 + \nu, \frac{D_{\rm max}}{D_n}\right) D_n^3 + B_2 \gamma\left(4 + \nu, \frac{D_{\rm max}}{D_n}\right) \times D_n^4 + B_3 \gamma\left(5 + \nu, \frac{D_{\rm max}}{D_n}\right) D_n^5. \tag{10}$$

*d. Continuous-collection growth equation with both the geometric sweep-out area and the terminal fall velocity corrections*

Using the gamma function (from the appendix) along with (5) and (8), one may derive continuous collection accounting for the oblateness of raindrops in both the geometric area term and terminal velocity term, resulting in

$$\frac{dq}{dt} = \frac{\pi E N_t q_c}{4\Gamma(\nu)} f_3 \left(\frac{\rho_{oo}}{\rho_o}\right)^{0.4}, \tag{11}$$

where

$$f_3 = (A_1^2 B_1)\gamma\left(3 + \nu, \frac{D_{\rm max}}{D_n}\right) D_n^3 + (A_1^2 B_2 + 2A_1 A_2 B_1)\gamma\left(4 + \nu, \frac{D_{\rm max}}{D_n}\right) D_n^4 + (A_1^2 B_3 + A_2^2 B_1 + 2A_1 A_2 B_2)\gamma \times \left(5 + \nu, \frac{D_{\rm max}}{D_n}\right) D_n^5 + (2A_1 A_2 B_3 + A_2^2 B_2)\gamma\left(6 + \nu, \frac{D_{\rm max}}{D_n}\right) D_n^6 + B_3 A_2^2 \gamma\left(7 + \nu, \frac{D_{\rm max}}{D_n}\right) D_n^7. \tag{12}$$

In (12) the coefficients can be combined and computed ahead of time for efficiency. Also, the partial gamma distributions in (10) and (12) can be found inexpensively using lookup tables.

*e. The Lin et al. (1983) evaporation equation for a generalized gamma distribution*

The LFO83 evaporation rate is derived here but with the assumption of a maximum diameter less than infinity, consistent with the other integration limits used in this paper. LFO83 and others derive the total evaporation rate for a population of drops by applying the appropriate ventilation coefficient to each nonventilated drop evaporation rate. Where they integrated over all drop diameters from 0 to ∞, we instead integrate from 0 to $D_{\rm max}$:

$$\frac{dq_r}{dt} = \frac{1}{\rho_o} \int_0^{D_{\rm max}} f_v(D) \frac{dm(D)}{dt} n_r(D)\, dD. \tag{13}$$

This solution is identical to the total evaporation rate for a drop population in a bin model. The original average vapor ventilation coefficient $f_v$ was defined by LFO83 as

$$f_v = 0.78 + 0.308 S_c^{1/3} N_{\rm RE}^{1/2} = 0.78 + 0.308 S_c^{1/3} [(V_{\rm eq} D_{\rm eq})/\nu]^{1/2}, \tag{14}$$

where $N_{\rm RE}$ is the Reynolds number, $S_c$ is the Schmidt number, and $\nu$ is the kinematic viscosity of air, from drop ventilation experiments of Beard and Pruppacher (1971; for $D_{\rm eq} < 0.8$ mm), which were later found to

[1] A similar polynomial was advocated by Rutledge and Hobbs (1983) but unfortunately was not adopted by the rest of the modeling community at the time. Also, it does not perform as well as the one we propose.

hold true for larger drops (Pruppacher and Rasmussen 1979; for $D_{eq} < 5$ mm). Also, K. V. Beard (2005, personal communication) argues that this ventilation formula can safely be extrapolated to sizes greater than 5 mm. LFO83 assume spherical drops using $D_{eq}$ for the length scale and use $V_{eq}$ from LO69 shown in (2). However, as discussed in section 2a, there is a problem with the LFO83 formulation affecting both the velocity and diameter in the ventilation term: LFO83 ignores that the larger drops are deformed.

Now, $dm(D)/dt$ in (13) is the nonventilated time rate of change of a drop's mass defined by Mason (1971, p. 123) as

$$\frac{dm(D)}{dt} = \frac{2\pi D(S-1)}{\left[\frac{L_v}{K_a T}\left(\frac{L_v}{R_v T} - 1\right) + \frac{R_v T}{e_s(T)\psi}\right]}, \quad (15)$$

where $D$ is drop diameter, $S$ is the saturation ratio, $L_v(T)$ is the latent heat of vaporization, $K_a$ is thermal conductivity of air, $\psi(T, P)$ is diffusivity of water vapor in air, $e_s(T)$ is the saturation vapor pressure over a plane surface of pure water, $R_v$ is the gas constant for water vapor, $T$ is air temperature, and $P$ is air pressure. In the denominator of (15), the first term is associated with the conduction of heat from the surrounding air and the second term is associated with vapor diffusion from the drop surface. This equation assumes that the raindrops are big enough that drop curvature does not play a role in evaporation. We can simplify the denominator of (15) by using the approximation $L_v/R_v T \gg 1$ and substituting the equation of state $e_s(T) = \rho_o q_{s,w} R_v T$:

$$\frac{dm(D)}{dt} = 2\pi D(S-1)\left(\frac{1}{\frac{L_v^2}{K_a R_v T^2} + \frac{1}{\rho_o q_{s,w}\psi}}\right). \quad (16)$$

To simplify temporarily, the variables that do not vary with particle diameter [rightmost expression in (16)] can be written as $G(T, P)$:

$$dm(D)/dt = 2\pi D(S-1)G(T, P).$$

Substituting the spectral density function [(A1)] and (14) and (15) into (13) gives

$$\frac{dq_r}{dt} = \frac{1}{\rho_o}\int_0^{D_{max}}\left[0.78 + 0.308 S_c^{1/3}\nu^{-1/2}a^{1/2}D^{(b+1)/2}\left(\frac{\rho_{oo}}{\rho_o}\right)^{0.2}\right]2\pi D(S-1)G(T, P)\frac{N_t}{\Gamma(\nu_r)}\left(\frac{D}{D_n}\right)^{\nu_r - 1}\exp\left(-\frac{D}{D_n}\right)\frac{dD}{D_n}, \quad (17)$$

which can be integrated, giving

$$\frac{dq_r}{dt} = \frac{2\pi(S-1)N_t D_n G(T, P)}{\rho_o \Gamma(\nu_r)}\left\{0.78\gamma\left(\nu_r + 1, \frac{D_{max}}{D_n}\right) + 0.308 S_c^{1/3}\nu^{-1/2}a^{1/2}D_n^{(b+1)/2}\gamma\left[\nu_r + \frac{(b+3)}{2}, \frac{D_{max}}{D_n}\right]\left(\frac{\rho_{oo}}{\rho_o}\right)^{0.2}\right\}. \quad (18)$$

This can be seen to be almost identical to LFO83 by plugging $\nu_r = 1$ and $D_{max} = \infty$ into (18), giving the familiar form

$$\frac{dq_r}{dt} = \frac{2\pi(S-1)N_t D_n}{\rho_o}\left[\frac{0.78\Gamma(2) + 0.308 S_c^{1/3}\nu^{-1/2}a^{1/2}D_n^{(b+1)/2}\Gamma\left(\frac{b+5}{2}\right)\left(\frac{\rho_{oo}}{\rho_o}\right)^{0.2}}{\frac{L_v^2}{K_a R_v T^2} + \frac{1}{\rho_o q_{s,w}\psi}}\right]. \quad (19)$$

### *f. Evaporation of raindrops with shape distortion included for a generalized gamma distribution*

Here a new raindrop evaporation rate equation is derived that accounts for shape distortion and uses a more appropriate length scale and fall velocity. Green (1975) proposed using a characteristic length scale $L$ in the Reynolds number calculation for raindrops and we follow suit except that, instead of assuming artificial oblate spheroid-shaped drops, we computed the drop surface areas and maximum perimeters from the greatly improved asymmetric drop model output shown in Beard and Chuang (1987) and applied those along with the observed raindrop fall speeds from PP71.

Skelland and Cornish (1963) found that the most relevant Reynolds number when investigating vapor transfer from oblate spheroids was one that used a characteristic dimension of length defined as

$$L = \frac{\text{Surface area}}{\text{maximum perimeter} \perp \text{flow}}.$$

Pasternak and Gauvin (1960) also found that this characteristic dimension $L$ was found to correlate the data between many different types of shapes from the literature (spheres, cylinders, disks, prisms, cubes, etc.) and therefore is the physically meaningful length scale when analyzing heat and mass transfer rates. It is easily

shown that $L$ is always less than $D_{eq}$ for an oblate or asymmetric spheroid shape and therefore acts to reduce the Reynolds number.

However, using the polynomial fit of the PP71 fall velocity [(8)], which accounts for increasingly deformed shape and drag (and reduced fall speed) of raindrops with size, reduces the Reynolds number by a greater amount than by using $L$ (not shown).

The revised ventilation term, reduced in magnitude by using both $V_T(D_{ob})$ and $L$, is

$$f_v = 0.78 + 0.308 S_c^{1/3} \nu^{-1/2} \left(\frac{\rho_{oo}}{\rho_o}\right)^{0.2} \times [(B_1 D_{eq} + B_2 D_{eq}^2 + B_3 D_{eq}^3) L]^{1/2}.$$

However, the problem is that this equation cannot be integrated. Therefore, we do a third-order fit on

$$[V_T(D_{ob}) L]^{1/2} = C_1 D_{eq} + C_2 D_{eq}^2 + C_3 D_{eq}^3,$$

where $C_1 = 70.306\ 276\ 1$, $C_2 = -7626.401\ 045\ 6$, and $C_3 = 347\ 907.833\ 921\ 6$. Plugging this result into the ventilation term gives a form that can be easily integrated:

$$f_v = 0.78 + 0.308 S_c^{1/3} \nu^{-1/2} \left(\frac{\rho_{oo}}{\rho_o}\right)^{0.2} \times (C_1 D_{eq} + C_2 D_{eq}^2 + C_3 D_{eq}^3). \quad (20)$$

Substitution of (20), (A1), and (16) into (13) and integrating give

$$\frac{dq_r}{dt} = \frac{2\pi (S-1) N_t D_n G(T,P)}{\rho_o \Gamma(\nu_r)} \left\{ 0.78 \gamma\left(\nu_r + 1, \frac{D_{max}}{D_n}\right) + 0.308 S_c^{1/3} \nu^{-1/2} \left(\frac{\rho_{oo}}{\rho_o}\right)^{0.2} \times \left[ \gamma\left(\nu_r + 2, \frac{D_{max}}{D_n}\right) C_1 D_n + \gamma\left(\nu_r + 3, \frac{D_{max}}{D_n}\right) C_2 D_n^2 + \gamma\left(\nu_r + 4, \frac{D_{max}}{D_n}\right) C_3 D_n^3 \right] \right\}. \quad (21)$$

This form is believed to be a more realistic raindrop evaporation equation because it includes the effects of how raindrop distortion reduces the ventilation/evaporation with increasing drop size.

## 3. Results and discussion

### a. Collection equation

To evaluate the continuous-collection growth equation, calculations are made for rain mixing ratios ranging from 1 to 15 g kg$^{-1}$, incremented by 1 g kg$^{-1}$, and number concentrations of 500 and 2000 m$^{-3}$ with the four derived continuous-collection formulas [(4), (6), (9), and (11)]. These cases of continuous-collection growth mixing ratio rate trends are shown in Figs. 3a and 3b. For these simulations we use the following parameters and constants: initial values for rain mixing ratio $q_r$ = 1–15 g kg$^{-1}$, diameter parameter $\beta = 3$, shape parameter $\nu = 3$ (values of 1, 2, and 4 were also tried but are not shown), constant rain concentration $N_t$ = 500 and 2000 m$^{-3}$, collection efficiency $E = 1$, density of water $\rho_w = 1000$ kg m$^{-3}$, $P = 100\ 000$ Pa, $T = 298$ K, $\rho_{ai}$ from the gas law (=1.17 kg m$^{-3}$), constant cloud water supply (such as within an updraft) $q_c = 1.0 \times 10^{-3}$ kg kg$^{-1}$, time step $\Delta t = 1$ s, and maximum diameter $D_{max} = 8$ mm.

The solutions for instantaneous continuous-collection rate calculations for rain mixing ratio amounts of 1–15 g kg$^{-1}$ and number concentrations of 500 and 2000 m$^{-3}$ are shown in Figs. 3a and 3b. For number concentrations of rain of 500 m$^{-3}$, the largest rates in descending order are with LFO terminal velocity (also known as LO69 terminal velocity) using oblate-like diameters. This result occurs because the terminal velocities and sweep-out diameters are largest in these calculations. Next, the standard LFO-type calculation parameters produce the second largest rates. These are followed by the new $O(3)$ terminal velocity and oblate-like diameter combination calculations. The small terminal velocities at larger sizes keep these values from exceeding those of the previous types of combinations of terminal velocities and diameters used in geometric sweep-out volumes. Last, the $O(3)$ terminal velocity values combined with equivalent diameters produce the smallest collection rates. For number concentration of 2000 m$^{-3}$ the solutions are much more tightly clustered (Fig. 3b) because the distributions are weighted toward smaller sizes for which differences between the oblate-like drops and spherical drops are less. In that $N_t$ = 2000 case, the new $O(3)$ terminal velocity and oblate-like diameter combination calculations have slightly faster accretion rates than those of LFO83. The most important difference to compare is that of the LFO83 parameterization and the new parameterization with oblate-like diameters and $O(3)$ terminal velocity computations. We are surprised at the smallness of the difference between solutions, but are comforted by the fact that most approximations give nearly similar solutions. The LFO-like method appears to come close to the more accurate oblate-like solution because of a can-

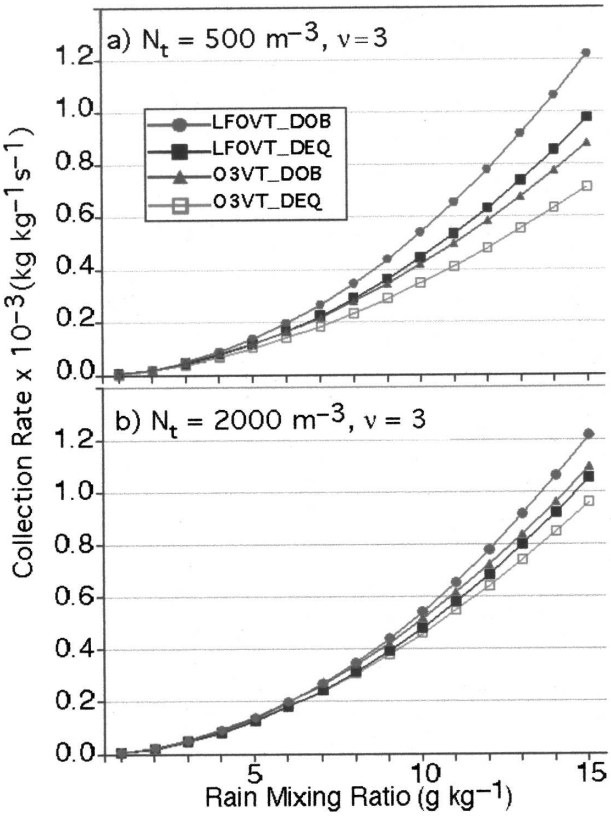


FIG. 3. Collection rate vs rain mixing ratio for (a) rain $N_t$ = 500 m$^{-3}$ and (b) rain $N_t$ = 2000 m$^{-3}$ for the four collection rate formulations: 1) equivalent diameter (DEQ) for geometric sweep-out area and LFO83 for terminal velocity (LFOVT) (solid squares), 2) oblate-like diameter (DOB) for geometric sweep-out area and LFO83 for terminal velocity (LFOVT) (solid circles), 3) equivalent diameter (DEQ) for geometric sweep-out area and $O(3)$ oblate-like terminal velocity (O3VT) (open squares), and 4) oblate-like diameter (DOB) for geometric sweep-out area and $O(3)$ oblate-like terminal velocity (O3VT) (solid triangles).

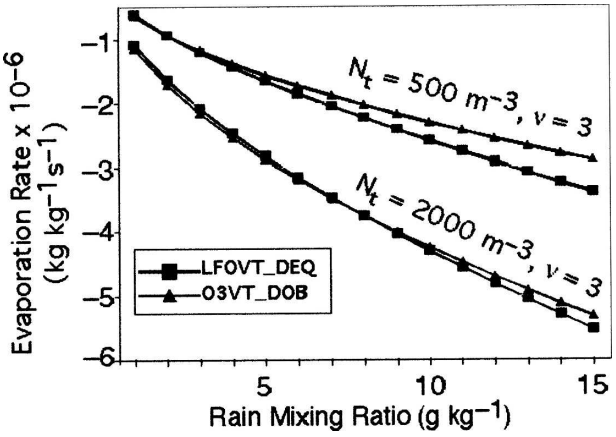


FIG. 4. Evaporation rates (kg kg$^{-1}$ s$^{-1}$) for LFO terminal velocity and equivalent diameters (LFO; squares) and $O(3)$ terminal velocity and oblate-like distorted diameters (OBLATE; triangles). Calculations with rain number concentrations of 500 and 2000 m$^{-3}$ are indicated.

cellation of two errors in its formulation: an erroneously small sweep-out diameter is compensated by an erroneously fast fall speed. This exercise may seem academic at this point, but it is important in that we now know how relevant it is to specify the more exact continuous-collection parameterization equation that accounts for oblate-like distortions.

### *b. Evaporation equation*

To evaluate the evaporation equations, solutions are computed for instantaneous rates with the two formulas (18) and (21). For these calculations we use the same parameters and constants as before but note the additional information that saturation ratio $S = 0.8$.

The solutions made for evaporation calculations for rain mixing ratio amounts of 1–15 g kg$^{-1}$ and number concentrations of 500 and 2000 m$^{-3}$ are shown in Fig. 4. Recall that we earlier showed that the $V_T$ term dominates differences that are seen in the evaporation rate equation between the LFO-like parameterization (19) and the new proposed distorted drop parameterization (21). For larger $N_t$ and small rain mixing ratio, the evaporation rate is slightly enhanced in the oblate-like distorted drop case [(21)] because the drop size distribution is weighted toward smaller drops that happen to fall faster (for $D < 3$ mm; Fig. 2). However, for any $N_t$ and larger mixing ratio, the oblate-like parameterization evaporates less, as expected, primarily because of reduced fall speeds and reduced ventilation. Furthermore, calculations with number concentrations of 500 m$^{-3}$ show a more significant spread between the LFO-like computations [(19)] and computations made with the oblate-like parameterization (21) than with number concentrations of 2000 m$^{-3}$. This situation is because the rain distributions are weighted toward larger sizes for the case of $N_t$ = 500 m$^{-3}$ in which the distortions from a sphere are greater.

## 4. Summary

In this paper it is shown that the use of oblate-like distortions in shapes of raindrops does not make a significant difference in some microphysical parameterizations such as continuous collection and evaporation. The biggest errors arise when more exact approximations (e.g., for distorted drop shape or oblate-like diameter) are not combined with appropriately sophisticated approximations for other variables dependent on drop shape and diameter (e.g., terminal velocity). For

this study, we propose a new terminal velocity formulation as well as new continuous-collection and evaporation parameterizations. All parameterizations and solutions were derived and computed using truncated distributions at diameters of 8 mm for raindrops. The results from this study show the following five results as compared with the LFO83-like solutions:

1) Continuous-collection rates are slightly larger ($N_t$ = 2000) or slightly smaller ($N_t$ = 500) using oblate-like diameters and the new $O(3)$ terminal velocity expression. Coincidental agreement owes to cancellation of two large errors in the LFO83-like solutions.
2) Evaporation rates are generally smaller using oblate-like diameters and the new terminal velocity expression, and differences in rates grow as the drop distribution is weighted toward larger sizes.
3) Solutions behaved similarly for various values of the distribution shape parameter $\nu$ for both continuous-collection and evaporation rates.
4) Although the exercise we went through in this paper came up with some complicated solutions for some parameterizations, we are comforted that what previously has been used or something akin to it gives reasonable results in comparison with these more sophisticated approaches.
5) The complicated expressions can be built up into lookup tables that make solutions available as quick as or more quickly than integrating equations from, say, LFO83.

The differences might seem small in these simple calculations, though their inclusion might be important in certain types of clouds such as Hawaiian rainbands and may have unexpected importance in other types of clouds as well. Future testing is needed of these improved microphysics parameterizations in cloud models to investigate their time-integrated impact. In addition, tests need to be done on rainfall rates with various approximations for terminal velocity. Although not done here, inspection suggests that the third-order approximation for terminal velocity presented herein as an alternative to the LO69/LFO83 terminal velocity approximation should produce smaller rainfall rates and should be more realistic. Last, though the results in this paper were intended for research models, we see no reason why, with the use of lookup tables, they could not be adopted for real-time prediction models.

*Acknowledgments.* This work was supported by the National Science Foundation under Grants ATM-0340693, ATM-0449753, and ATM-0339519. Doctor Kenneth V. Beard gave helpful advice on computing accurate surface areas of his asymmetric drops and provided many useful constructive criticisms to improve this paper. To him we are most thankful.

## APPENDIX

### Description of Spectral Density Function and Distribution Moments

The spectral density function in this study is given by the gamma distribution. This function has been used by Walko et al. (1995), Meyers et al. (1997), and Cohard and Pinty (2000), among many others, and is given by

$$n(D) = \frac{N_t}{\Gamma(\nu)} \frac{1}{D_n} \left(\frac{D}{D_n}\right)^{\nu-1} \exp\left(-\frac{D}{D_n}\right), \quad \text{(A1)}$$

where $D$ is diameter (m), $D_n$ is the characteristic diameter (m), $N_t$ is total number concentration (zeroth moment; $m^{-3}$) given by

$$N_t = \int_0^{D_{\max}} n(D)\, dD,$$

$\nu$ is a distribution shape parameter (dimensionless), and $\Gamma$ is the complete gamma function, where $\Gamma(\nu + 1) = \nu\Gamma(\nu)$.

The third moment, or mixing ratio $q$ (kg $kg^{-1}$), can be defined over the interval $D(0, D_{\max})$ by

$$q = \frac{1}{\rho_o} \int_0^{D_{\max}} m(D)n(D)\, dD = \frac{\alpha N_t \gamma\left(\beta + \nu, \frac{D_{\max}}{D_n}\right)}{\rho_o \Gamma(\nu)} D_n^{\beta}, \quad \text{(A2)}$$

where $\gamma$ is the partial gamma function integrated from 0 to $D_{\max}$. In all of the equations, for spheres, the mass is given by $m(D) = \alpha D^{\beta}$, where $\alpha = \rho\pi/6$ and $\beta = 3$. After rearranging (A2), the variable $D_n$ can be found in terms of $N_t$ and $q$ and other constants using an iterative form of

$$D_n = \left[\frac{q\rho_o\Gamma(\nu)}{\alpha N_t \gamma\left(\beta + \nu, \frac{D_{\max}}{D_n}\right)}\right]^{1/\beta}. \quad \text{(A3)}$$

## REFERENCES

Andsager, K., K. V. Beard, and N. F. Laird, 1999: Laboratory measurements of rain axis ratios for large raindrops. *J. Atmos. Sci.,* **56,** 2673–2683.

Beard, K. V., 1976: Terminal velocity and shape of cloud and precipitation drops aloft. *J. Atmos. Sci.,* **33,** 851–864.

——, and H. R. Pruppacher, 1969: A determination of terminal velocity and drag of small drops by means of a wind tunnel. *J. Atmos. Sci.,* **26,** 1066–1072.

——, and ——, 1971: A wind tunnel investigation of the rate of

evaporation of small water droplets falling at terminal velocity in air. *J. Atmos. Sci.,* **28,** 1455–1464.
——, and C. Chuang, 1987: A new model for the equilibrium shape of raindrops. *J. Atmos. Sci.,* **44,** 1509–1524.
Bringi, V. N., and V. Chandrasekar, 2000: *Polarimetric Doppler Weather Radar: Principles and Applications*. Cambridge University Press, 636 pp.
Cohard, J.-M., and J.-P. Pinty, 2000: A comprehensive two-moment warm microphysical bulk scheme, I: Description and tests. *Quart. J. Roy. Meteor. Soc.,* **126,** 1815–1842.
Gilmore, M. S., J. M. Straka, and E. N. Rasmussen, 2004: Precipitation and evolution sensitivity in simulated deep convective storms: Comparisons between liquid-only and simple ice and liquid phase microphysics. *Mon. Wea. Rev.,* **132,** 1897–1916.
Green, A. W., 1975: An approximation for the shapes of large raindrops. *J. Appl. Meteor.,* **14,** 1578–1583.
Gunn, R., and G. D. Kinzer, 1949: The terminal velocity of fall for water drops in stagnant air. *J. Meteor.,* **6,** 243–248.
Lin, Y.-L., R. Farley, and H. D. Orville, 1983: Bulk parameterization of the snow field in a cloud model. *J. Climate Appl. Meteor.,* **22,** 1065–1092.
Liu, Y., and H. D. Orville, 1969: Numerical modeling of precipitation and cloud shadow effects on mountain-induced cumuli. *J. Atmos. Sci.,* **26,** 1283–1298.
Mason, B. J., 1971: *The Physics of Clouds*. 2d ed. Oxford University Press, 671 pp.
Meyers, P. M., R. L. Walko, J. Y. Harrington, and W. R. Cotton, 1997: New RAMS cloud physics parameterization. Part II: The two-moment scheme. *Atmos. Res.,* **45,** 3–39.
Pasternak, I. S., and W. H. Gauvin, 1960: Turbulent heat and mass transfer from stationary particles. *Can. J. Chem. Eng.,* **38,** 35–42.
Pruppacher, H. R., and K. V. Beard, 1970: A wind tunnel investigation of the internal circulation and shape of water droplets falling at terminal velocity in air. *Quart. J. Roy. Meteor. Soc.,* **96,** 247–256.
——, and R. L. Pitter, 1971: A semi-empirical determination of the shape of cloud and rain drops. *J. Atmos. Sci.,* **28,** 86–94.
——, and R. Rasmussen, 1979: A wind tunnel investigation of the rate of evaporation of large water drops falling at terminal velocity in air. *J. Atmos. Sci.,* **36,** 1255–1260.
——, and J. D. Klett, 1997: *Microphysics of Clouds and Precipitation*. Kluwer Academic, 954 pp.
Rauber, R. M., K. V. Beard, and B. M. Andrews, 1991: A mechanism for giant raindrop formation in warm, shallow convective clouds. *J. Atmos. Sci.,* **48,** 1791–1797.
Reisner, J., R. M. Rasmussen, and R. T. Bruintjes, 1998: Explicit forecasting of supercooled liquid water in winter storms using the MM5 mesoscale model. *Quart. J. Roy. Meteor. Soc.,* **124,** 1071–1107.
Rutledge, S. A., and P. V. Hobbs, 1983: The mesoscale and microscale structure and organization of clouds and precipitation in midlatitude cyclones. VIII: A model for the "seeder-feeder" process in warm-frontal rainbands. *J. Atmos. Sci.,* **40,** 1185–1206.
Skelland, A. H. P., and A. R. H. Cornish, 1963: Mass transfer from spheroids to an air stream. *AIChE J.,* **9,** 73–76.
Thompson, G., R. M. Rasmussen, and K. Manning, 2004: Explicit forecasts of winter precipitation using an improved bulk microphysics scheme. Part I: Description and sensitivity analysis. *Mon. Wea. Rev.,* **132,** 519–542.
Walko, R. L., W. R. Cotton, M. P. Meyers, and J. Y. Harrington, 1995: New RAMS cloud physics parameterization. Part I: The single-moment scheme. *Atmos. Res.,* **38,** 3–39.